

Accelerated robust optimization algorithm for proton therapy treatment planning.

Gregory Buti¹, Kevin Souris¹, Ana M. Barragán Montero¹, Marie Cohilis¹, John A. Lee¹, Edmond Sterpin^{1,2}

¹Université Catholique de Louvain, Institut de Recherche Expérimentale et Clinique (IREC), Center of Molecular Imaging, Radiotherapy and Oncology (MIRO), Brussels, Belgium

²Katholieke Universiteit Leuven, Department of Oncology, Laboratory of Experimental Radiotherapy, Leuven, Belgium

Version typeset February 12, 2020

E-mail: gregory.butl@uclouvain.be

Abstract

Purpose: Robust optimization is a computational expensive process resulting in long plan computation times. This issue is especially critical for moving targets as these need a large number of uncertainty scenarios to robustly optimize their treatment plans. In this study, we propose a novel worst-case robust optimization algorithm, called dynamic minimax, that accelerates the conventional minimax optimization. Dynamic minimax optimization aims at speeding up the plan optimization process by decreasing the number of evaluated scenarios in the optimization.

Methods: For a given pool of scenarios (for instance $63 = 7 \text{ setup} \times 3 \text{ range} \times 3 \text{ breathing phases}$), the proposed dynamic minimax algorithm only considers a reduced number of candidate-worst scenarios, selected from the full 63 scenario set. These scenarios are updated throughout the optimization by randomly sampling new scenarios according to a hidden variable P , called the ‘probability acceptance function’, which associates with each scenario the probability of it being selected as the worst case. By doing so, the algorithm favors scenarios that are mostly “active”, that is, frequently evaluated as the worst case. Additionally, unconsidered scenarios have the possibility to be re-considered, later on in the optimization, depending on the convergence towards a particular solution.

The proposed algorithm was implemented in the open-source robust optimizer MIROpt and tested for [six 4D-IMPT lung tumor patients with various tumor sizes](#)

32 **and motions.** Treatment plans were evaluated by performing comprehensive robust-
33 ness tests (simulating range errors, systematic setup errors and breathing motion) using
34 the open-source Monte-Carlo dose engine MCsquare.

35 **Results:** The dynamic minimax algorithm achieved an optimization time gain of 84%,
36 on average. The dynamic minimax optimization results in a significantly noisier opti-
37 mization process due to the fact that more scenarios are accessed in the optimization.
38 However, the increased noise level does not harm the final quality of the plan. In fact,
39 the plan quality is similar between dynamic and conventional minimax optimization
40 with regards to target coverage and normal tissue sparing: on average, the difference
41 in worst-case D95 is 0.2 Gy and the difference in mean lung dose and mean heart dose
42 is 0.4 Gy and 0.1 Gy, respectively (evaluated in the nominal scenario).

43 **Conclusions:** The proposed worst-case 4D-robust optimization algorithm achieves a
44 significant optimization time gain of 84%, without compromising target coverage or
45 normal tissue sparing.

46 **Keywords**— proton therapy, robust optimization, minimax

1. Introduction

The superior dose distributions produced by intensity-modulated proton therapy (IMPT) indicate a potential for improved patient outcome as compared to conventional X-ray radiotherapy.^{1,2,3} However, it is of critical importance that the IMPT treatment plan is made sufficiently robust in order to prevent an unacceptable deterioration of the treatment at the moment of delivery. Successful treatment planning strategies must therefore take into account treatment uncertainties such as tumor motion, setup and range errors.^{4,5,6,7} In proton therapy treatment planning, the most effective way of handling these uncertainties is to simulate them during the plan optimization process. This approach has led to the development of robust optimization algorithms which provide an alternative to more conventional margin-based approaches.^{8,9,10,11}

In general, the different robust optimization algorithms can be classified into two main groups: (1) probabilistic (or stochastic) optimization and (2) worst-case robust optimization.^{12,13} Both groups aim at covering treatment uncertainties by simulating a discrete set of treatment uncertainty scenarios (i.e., realizations of specific combinations of treatment errors). However, the algorithms differ in the way in which the objective function is minimized. Probabilistic optimization algorithms minimize the expected value of the objective function. In contrast, in worst-case robust optimization, the worst-case scenario (the one with the highest objective function value) is chosen, at each iteration, to minimize the objective function.

In this study, we focus on worst-case robust optimization. Different approaches for worst-case robust optimization have been proposed, depending on the way the worst-case scenario is defined. For instance, in voxel-wise worst-case optimization, the worst-case scenario is defined by considering the worst-case value for each individual voxel, among all scenarios (i.e., high dose in organ-at-risk voxels and low dose in the target voxels).^{8,9} However, this approach results in a non-physical and potentially overly conservative solution.^{10,14} For this reason, Fredriksson *et. al* introduced the so-called ‘minimax’ optimization where, for each uncertainty scenario, the objective function is computed for all voxels simultaneously.¹⁰ Minimax optimization for IMPT treatment plans have shown to yield clinically acceptable target coverage, in the presence of treatment uncertainties, for a variety of tumor locations.^{15,16} The main drawback of both minimax and voxel-wise worst-case optimization is their computationally expensive nature, both in terms of the plan computation time and memory consumption. This is due to the following two main issues: first, dose-influence

77 matrices must be computed and stored for each treatment uncertainty scenario and second, dose
78 distributions must be re-evaluated, at each iteration, for all scenarios defined within the uncertainty
79 set. Because the uncertainty sources (such as tumor motion, setup error and range errors) are
80 usually handled in a mutually independent way, moving targets are especially resource demanding,
81 as their increased number of uncertainty sources amount to a large number of scenarios. This limits
82 the potential of minimax optimization as a standard clinical tool and prevents its applicability in
83 online-adaptive workflows.¹⁷

84 An example of an approach that aims at reducing the plan computation time is to reduce the
85 number of uncertainty scenarios, with the goal of limiting the number of scenario evaluations during
86 optimization. To this end, in a previous study, a planning strategy was proposed that pre-selects
87 a reduced set of relevant uncertainty scenarios, resulting in a significant plan computation time
88 gain.¹⁸ In contrast, in this study, the full pre-defined uncertainty set is maintained, but we propose
89 an approximate ‘*dynamic*’ minimax algorithm that deals with the inherently long optimization
90 time of the conventional minimax optimization algorithm. We focus on accelerating minimax
91 optimization by considering only a reduced set of scenarios, selected from the full uncertainty set.
92 This reduced set is then dynamically updated throughout the optimization process, in order to
93 retain only those scenarios that are mostly active in guiding the optimization solution. The present
94 study aims to address the feasibility of this *dynamic* minimax optimization and analyses the time
95 gain with respect to *conventional* minimax. In order to illustrate the proposed method, [six](#) lung
96 cancer patients [with various tumor sizes and motions](#) are used.

97 II. Material and Methods

98 In this section, first, the *conventional* minimax optimization algorithm is formalized, followed by
99 a detailed presentation of the proposed *dynamic* minimax optimization algorithm. Afterwards, an
100 overview is given of the optimization software and patient data used for the testing and evaluation
101 of the respective methods.

102 II.A. Conventional Minimax Optimization

103 By representing S as the pre-defined set of uncertainty scenarios s , *conventional* minimax opti-
104 mization is typically formulated as:

$$105 \quad \min_w \max_s \{f_{obj}(d(w, s))\} \quad (1)$$

$$106 \quad \text{s.t.} \quad \begin{cases} w \geq 0 \\ s \in S, \end{cases}$$

107

108 with f_{obj} as the objective function, d the dose distribution and w the optimization variables (i.e.,
109 the spot weights) which are constrained to allow only positive solutions. The *conventional* minimax
110 algorithm is characterized by the following three steps performed at each iteration of optimization:
111 (1) the dose distribution is computed for all scenarios s in S with the objective function f_{obj}
112 evaluated in each of the scenarios, (2) the worst-case scenario is selected as the scenario in which
113 the objective function attains its highest value and (3) the spot weights w are updated by minimizing
114 the objective function of the current worst-case scenario.

115 II.B. Dynamic Minimax Optimization

116 The proposed algorithm differs from the *conventional* minimax optimization algorithm by de-
117 composing the pre-defined uncertainty set S into two scenario pools: (1) an ‘active pool’ S_A of
118 candidate-worst scenarios (the pool size of S_A is denoted as N_A) and (2) a ‘dead pool’ S_D contain-
119 ing the leftover scenarios (the number of dead pool scenarios is denoted as N_D). Hence, the union
120 of both pools is equal to S ($S_A \cup S_D = S$). From this point onward, we denote the active pool
121 scenarios and dead pool scenarios as ‘active scenarios’ and ‘dead scenarios’, respectively. The idea
122 is to identify the scenarios that are mostly used in guiding the optimization solution and include
123 these scenarios into the active pool S_A . Subsequently, at each iteration, only the active scenarios
124 ($s \in S_A$) are considered. Hence, the *dynamic* minimax algorithm can be re-formulated as follows:

$$125 \quad \min_w \max_s \{f_{obj}(d(w, s))\}$$

$$126 \quad \text{s.t.} \quad \begin{cases} w \geq 0 \\ s \in S_A. \end{cases}$$

127

128 The active scenarios ($s \in S_A$) are probabilistically selected, based on an auxiliary variable P , the
129 so-called ‘acceptance probability set’ $P = \{P_s \mid s \in S\}$ which associates with each scenario the

130 probability that it might be evaluated as the worst case.¹ P serves a similar role to the acceptance
 131 probability function commonly found in simulated annealing optimization schedules.¹⁹ Because P
 132 plays a key role in the *dynamic* minimax algorithm, we explain in the following two paragraphs (1)
 133 how P is updated over time and (2) how active scenarios are subsequently selected from P .

134 II.B.1. Acceptance probability set P

135 At each iteration, the acceptance probability P is updated by performing two steps. In the first
 136 step, the value P_s of the current worst-case scenario ($s = s_{worst}$) is incremented by a factor $\alpha(t)$:

$$137 \quad P_s(t) = P_s(t-1) + \alpha(t) \text{ if } s = s_{worst}, \quad (2)$$

138 followed by a re-normalization of P :

$$139 \quad P_s(t) = P_s(t) \times \frac{1}{1 + \alpha(t)} \quad \forall s \in S, \quad (3)$$

140 with t the iteration number and $\alpha(t)$ a global time-varying parameter. Following simulated anneal-
 141 ing optimization, $\alpha(t)$ is chosen to decay over time and is defined as $\alpha(t) = 1/t$. In doing so, P
 142 gradually reduces its sensitivity to fluctuations in the optimization process (so-called optimization
 143 noise). In the second step, the values P_s of the current dead scenarios ($s \in S_D$) are incremented
 144 by a factor $\alpha(t)/N_D$:

$$145 \quad P_s(t) = P_s(t-1) + \frac{\alpha(t)}{N_D} \quad \forall s \in S_D(t), \quad (4)$$

146 again followed by a re-normalization of P :

$$147 \quad P_s(t) = P_s(t) \times \frac{1}{1 + \alpha(t)} \quad \forall s \in S. \quad (5)$$

148 Step 2 is performed in order to add the possibility that yet unconsidered (i.e., dead) scenarios may
 149 become active at a later point in the optimization. In Eq. 4, $\alpha(t)$ is weighted by the size of the
 150 dead pool, ensuring that a worst-case evaluation (Eq. 2) weights more than its absence from the
 151 active pool. The re-normalization steps of P (Eqs. 3 and 5) are necessary to maintain at all times,
 152 a total probability mass of 1 (see Section II.B.2.). Additionally, they serve to effectively reduce the
 153 values of inactive scenarios (that is, scenarios present in the active pool but not contributing to the
 154 optimization) so that these can eventually be discarded.

¹It must be noted that this scenario ‘probability’ P_s does not bear a resemblance with the uncertainty probability of the scenario, typically used in probabilistic optimization.

155 II.B.2. Active pool S_A

156 Throughout the optimization process, the active pool scenarios are selected by randomly sampling
157 (without replacement), N_A number of scenarios according to their probabilities specified in P . In
158 other words, each scenario can only be drawn once, with the probabilities in P normalized after
159 each draw, in order to maintain a probability mass of 1.

160 In practice, the active pool is updated at discrete points during the optimization process (in
161 our case at an iteration interval of $\Delta t = 10$). At the start, P is initialized by assigning a uniform
162 probability distribution with no scenarios left unconsidered (i.e., all scenarios $s \in S$ are evaluated).
163 After the first active pool update, the active pool size is set to its reduced size and active scenarios
164 will be selected using the method described above. Furthermore, because some planning objectives
165 (typically the OAR dose constraints) are evaluated in the nominal scenario only, the nominal
166 scenario is always included active pool throughout the entire optimization process.

167 In general, the *dynamic* minimax algorithm is characterized by the size of the active pool
168 N_A , which is a user-defined parameter. In Section III., we will investigate how the choice of N_A
169 influences the resulting optimization process.

170 II.C. Optimization Software

171 The proposed *dynamic* minimax algorithm was implemented in the open-source treatment plan-
172 ning system MIROpt, coded in Matlab (MathWorks, Natick, United States).^{20,21} MIROpt uses
173 the open-source Monte Carlo dose engine MCsquare for its dose calculations (MCsquare has been
174 validated for clinical practice from commissioning measurements).^{22,23} Dose calculations are per-
175 formed with 10^5 ions per spot on a $2 \times 2 \times 2$ mm³ dose grid and the spot weights are optimized
176 using a gradient descent algorithm. Constraints on the optimization variable (spot weights w) are
177 handled by a simple projection method, that is, negative values of w are projected to the admissible
178 solution space by setting their values to zero. In order to compare the optimization times of the dif-
179 ferent optimization algorithms, the maximum number of iterations obtained from the *conventional*
180 minimax optimization is subsequently used in the *dynamic* minimax optimizations.

181 A quadratic objective function is used to penalize deviations from the pre-defined treatment
182 planning objectives. As would be performed conventionally in clinical practice, only the target
183 planning objectives were handled robustly (i.e., evaluated for all considered uncertainty scenarios)

184 whilst the OAR objectives were evaluated in the nominal scenario only. Plan optimization was
185 performed on a 256GB RAM system with a 2x8 Core Intel Xeon processor (E5-2667 v3) @3.20
186 GHz.

187 For the *dynamic* minimax optimizations, both the objective functions in the ‘approximate’ (= *proxy*)
188 worst-case scenario (i.e., the worst-case scenario evaluated only for the active pool scenarios)
189 and the ‘exact’ worst-case scenario (i.e., evaluated for all uncertainty scenarios) will be reported
190 in the results Section III. The former is, from this point onward, denoted as the ‘*proxy* worst-case
191 scenario’ and the latter as the ‘*exact* worst-case scenario’. Generally, in the *dynamic* minimax
192 optimization, the *exact* worst-case scenario is unavailable as not all uncertainty scenarios are eval-
193 uated at each iteration. However, in order to compare the different methods, additional *dynamic*
194 minimax optimizations are performed where all uncertainty scenarios are evaluated, storing the
195 objective function in the *exact* worst-case scenario as well.

196 II.D. Robustness Evaluation

197 The robustness of all resulting plans was evaluated with MCsquare, by using a comprehensive
198 approach in which the dose distribution is recomputed on a set of 250 treatment error *evaluation*
199 scenarios. These *evaluation* scenarios include effects of systematic setup errors, range errors and
200 respiratory motion.²⁴ Setup errors and range errors are sampled from normal distributions with
201 a standard deviation of 2 mm and 1.6%,²⁵ respectively, whilst respiratory motion is modeled by
202 recomputing the dose on each breathing phase CT and accumulating the dose on the reference (time-
203 averaged mid-position (MidP)) CT.²⁶ A 90% confidence interval is generated in the dosimetric space
204 by discarding the 10% worst scenarios (based on the target D_{95}) of the above-mentioned 250 error
205 scenarios.²⁴ The number of protons is selected in order to reach a statistical uncertainty of 1%.

206 For the dosimetric plan evaluations, the target DVH metrics (CTV D_{95} and CTV D_5) are
207 calculated in the worst-case *evaluation* scenario, i.e., the scenario where the lowest target coverage
208 is realized (based on CTV D_{95}), within the 90% confidence interval generated using the method
209 mentioned above. In the results section (Section III.), this worst-case *evaluation* scenario will be
210 referred to as the ‘*tested* worst-case scenario’, in order to draw a distinction between the worst-case
211 scenarios used throughout the optimization process (i.e., the *proxy* and *exact* worst-case scenarios)
212 and the worst-case scenario used for the robustness evaluation (i.e., the *tested* worst-case scenario).
213 The CTV bandwidths (BW) at the D_{95} and D_5 dose levels, are calculated within the same 90%

214 confidence interval. In other words, the BW represents the difference in dose between the *tested*
215 best-case and *tested* worst-case scenario, at a given dose level. The OAR DVH metrics will be
216 calculated in the nominal scenario only, meaning that the dose distribution is recomputed on the
217 nominal planning CT with a statistical uncertainty of 1%.

218 II.E. Patient Cases

219 Six lung tumor patients were chosen to test the proposed optimization algorithm, as their treatment
220 planning typically involves a large number of optimization scenarios, causing long plan optimization
221 times. Patient data were characterized by a 4D-CT image set, binned in ten breathing phases,
222 evenly spaced in time. All patients presented a single tumor volume, delineated on the MidP-
223 CT. The main features of the patient cohort are summarized in Table 1. All patients had a
224 dose prescription of 60 Gy to the clinical-target-volume (CTV) with target coverage considered
225 acceptable if 95% of the CTV received more than 95% of the prescribed dose (= 57 Gy), whilst no
226 more than 5% of the CTV received over 105% of the prescribed dose (= 63 Gy), for the worst-case
227 scenario.

228 All treatment plans used the MidP-CT as the nominal planning CT which was created with
229 the open-source platform OpenReggui.^{26,27} Treatment plans were optimized using uncertainty
230 scenarios that contain setup errors, range errors and respiratory motion. Similar to other studies,
231 uncertainty parameters were chosen as combinations of 5 mm setup errors in the three directions
232 (left-right, anterior-posterior and superior-inferior), $\pm 3\%$ range error and maximum inhale and
233 exhale breathing phases, generating an uncertainty set of 63 scenarios (= 7 setup error scenarios
234 \times 3 range error scenarios \times 3 breathing phases).^{6,8,10,28} Setup and range errors are modeled by
235 rigidly shifting the CT image and uniformly scaling the CT mass densities (obtained from the CT
236 image), respectively. All treatment plans were designed using a configuration of three co-planar
237 beams, delivered via IMPT with the pencil beam scanning (PBS) technique (see Table 1).

Table 1: Patient characteristics.

Patient	CTV size [cm ³]	Motion Amplitude			Tumor position	Beam angles [°]
		LR [mm]	AP [mm]	SI [mm]		
P1	152.6	4.2	2.1	3.1	RML	0, 270, 310
P2	107.7	3.1	2.9	3.7	LLL	90, 135, 180
P3	41.3	1.4	2.9	0.8	RUL	180, 225, 270
P4	70.3	0.8	1.2	0.5	LUL	90, 135, 180
P5	109.6	2.2	1.8	6.6	RUL	180, 225, 270
P6	249.7	2.1	2.5	10.6	RLL	180, 225, 270

Tumor motion amplitude (in left-right (LR), anterior-posterior (AP) and superior-inferior (SI) directions). Tumor positions (right-middle lobe (RML), left-lower lobe (LLL), right-upper lobe (RUL), right-lower lobe (RLL) and left-upper lobe (LUL)).

III. Results

In this section, the performance of *dynamic* minimax optimization algorithm is compared to the *conventional* minimax optimization. As mentioned in Section II., the *conventional* minimax algorithm evaluates, at each iteration, all 63 scenarios in the uncertainty set. Because the *dynamic* minimax is characterized by the parameter N_A , we present the results for two different choices of N_A , that is, $N_A = 15$ and a more extreme case of $N_A = 5$. The performance of the optimizations will be assessed by the achieved time-gain and the resulting plan quality. The plan quality is measured first, according to the value of the worst-case objective function value throughout the optimization process (so-called optimization curve) and second, from the dosimetric metrics (target coverage, robustness and OAR sparing) obtained after performing comprehensive robustness evaluations (see Section II.D.).

III.A. Optimization Data Results

Table 2 reports the plan optimization times, together with the final (worst-case) objective function value f . For the *dynamic* minimax optimization, the final objective function values f_{proxy} and f_{exact} are reported, which represent the objective function evaluated in the *proxy* worst-case and the *exact* worst-case scenario, respectively (see Section II.C.). Because the *conventional* minimax optimization evaluates, by default, all uncertainty scenarios, its final worst-case objective function

255 value is denoted as f_{exact} in Table 2. Results show that the *dynamic* minimax algorithm achieved
 256 an average time gain of 84% and 67%, for the 5 and 15 active pool size optimizations, respectively.
 257 The final objective function values of the different optimization methods are similar in magnitude
 258 for all test cases, with only a small difference between f_{proxy} and f_{exact} .

259 In Fig. 1 (top and middle panels), the optimization curves of the three optimizations (*conven-*
 260 *tional* minimax, $N_A = 15$ and $N_A = 5$ *dynamic* minimax) are compared. All optimizations follow
 261 a similar trend but with the $N_A = 5$ optimization lying below the *conventional* throughout the
 262 entire optimization process. The $N_A = 5$ optimization does appear to be significantly the noisiest.
 263 Fig. 1 (middle) shows that the *proxy* worst-case optimization curve of the $N_A = 5$ optimization
 264 deviates slightly from the *exact* worst-case optimization curve during an early stage but reaches
 265 similar values near the end of the optimization process.

266 Fig. 1 (bottom) shows the number of iterations that a scenario (ordered from 1 to 63) is selected
 267 as the worst case. Although mostly similar, the *conventional* minimax optimization accessed the
 268 least amount of scenarios, in order to reach its final solution. In contrast, the *dynamic* minimax
 269 optimizations use a larger number of rarely accessed scenarios with the bigger pool size *matching*
 270 *closely* the *conventional* minimax optimization.

Table 2: Plan optimization time, final worst-case objective function values f_{proxy} (evaluated only for the active pool scenarios) and f_{exact} (evaluated for all scenarios). Plans of each patient (P1-6) were obtained using the *conventional* minimax optimization (Ref.) and *dynamic* minimax optimization algorithms with pool sizes of $N_A=5$ and $N_A=15$. The average time reductions (in %) are reported at the bottom.

	Optimization time [min]			Final f_{exact}			Final f_{proxy}	
	Ref.	$N_A=15$	$N_A=5$	Ref.	$N_A=15$	$N_A=5$	$N_A=15$	$N_A=5$
P1	513	170	85	1.55	1.45	1.27	1.43	1.08
P2	396	142	72	0.74	0.63	0.69	0.61	0.55
P3	167	47	22	1.96	1.79	2.24	1.78	1.63
P4	219	79	32	2.97	2.57	3.02	2.50	1.71
P5	409	152	83	1.02	0.98	1.07	0.93	0.73
P6	758	213	107	6.0	5.3	4.8	5.3	4.4
ΔAvg.		-67%	-84%					

271 III.B. Dosimetric Results

272 Table 3 and Table 4 show the target and OAR DVH metrics for the obtained treatment plans.
273 Target coverage metrics (D_{95} and D_5) are calculated in the *tested worst-case scenario* whilst the
274 OAR metrics are *calculated in the nominal scenario only* (see Section II.D.). Furthermore, the
275 average difference between the value in the reference plan (obtained using *conventional* minimax
276 optimization algorithm) with plans optimized using the *dynamic* minimax algorithms is shown for
277 each metric.

278 On average, equal target coverage (worst-case CTV D_{95}) is obtained between the *conventional*
279 minimax and $N_A = 15$ *dynamic* minimax optimization. The $N_A = 5$ *dynamic* minimax optimiza-
280 tion improved worst-case CTV D_{95} slightly by 0.2 Gy, on average, with respect to the reference
281 plans. OAR dose is similar between all studied plans (average difference of mean lung dose of
282 only 0.2 Gy and 0.4 Gy between the *conventional* minimax and $N_A = 15$ and $N_A = 5$ *dynamic*
283 minimax optimizations, respectively and difference in mean esophagus dose of -0.1 Gy and 0.1 Gy,
284 respectively).

285 Fig. 2 displays the dose distribution together with the corresponding DVHs for each optimiza-
286 tion method. Results indicate similar dose profiles between all plans with isodose lines that nearly
287 coincide. This similarity translates to DVHs that have a similar sensitivity to the treatment errors
288 (indicated by the CTV BWs in Table 3) and matching OAR DVH curves.

Table 3: Target coverage metrics (CTV D_{95} and D_5) and robustness metrics (CTV bandwidth (BW) at the D_{95} and D_5 dose level) for plans of all patients (P1-6), obtained using *conventional* minimax (Ref.) and *dynamic* minimax optimization with pool sizes of $N_A=5$ and $N_A=15$. CTV D_{95} and D_5 are computed in the *tested* worst-case scenario.

CTV						
	Worst-case D_{95} [Gy]			Worst-case D_5 [Gy]		
	Ref.	$N_A=15$	$N_A=5$	Ref.	$N_A=15$	$N_A=5$
P1	57.0	56.9	57.3	62.8	62.4	62.4
P2	57.6	57.6	57.3	61.8	61.8	61.7
P3	58.0	57.9	58.5	62.6	62.6	61.9
P4	58.2	58.3	58.6	62.1	62.1	62.4
P5	58.3	58.4	58.5	61.7	61.7	61.6
P6	57.2	57.4	57.2	64.2	63.6	63.6
ΔAvg.		0.0	+0.2		-0.2	-0.3
	BW at D_{95} [Gy]			BW at D_5 [Gy]		
	Ref.	$N_A=15$	$N_A=5$	Ref.	$N_A=15$	$N_A=5$
P1	1.9	1.8	1.5	1.1	0.9	1.0
P2	1.1	0.9	0.9	0.9	0.8	0.8
P3	0.6	0.8	0.3	1.1	1.2	1.4
P4	0.6	0.6	0.4	1.0	1.0	1.4
P5	0.6	0.5	0.4	0.6	0.7	0.5
P6	1.6	1.5	1.7	1.6	1.6	1.6
ΔAvg.		-0.1	-0.2		0.0	+0.1

Table 4: Organ-at-risk DVH metrics (lung, esophagus and heart) for plans of all patients (P1-6), obtained using *conventional* minimax (Ref.) and *dynamic* minimax optimization with pool sizes of $N_A=5$ and $N_A=15$. Metrics have been computed in the nominal scenario.

	Lung						Esophagus			Heart		
	V_{20} [%]			D_{mean} [Gy]			D_{mean} [Gy]			V_{40} [%]		
	Ref.	$N_A=15$	$N_A=5$	Ref.	$N_A=15$	$N_A=5$	Ref.	$N_A=15$	$N_A=5$	Ref.	$N_A=15$	$N_A=5$
P1	26.4	26.5	28.3	13.5	13.6	14.1	2.0	2.0	2.1	3.2	3.3	3.4
P2	26.9	27.2	27.8	13.5	13.6	13.9	5.4	5.5	5.7	3.8	3.9	4.0
P3	13.4	13.4	13.6	7.0	7.0	7.2	4.8	4.8	5.0	0.0	0.0	0.0
P4	19.0	19.1	19.4	9.7	9.8	10.0	2.1	2.1	2.2	0.0	0.0	0.0
P5	21.9	22.1	22.4	10.6	10.8	10.9	7.9	8.0	8.3	1.1	1.2	1.2
P6	30.0	31.6	31.6	16.0	16.6	16.6	20.3	19.7	19.7	3.3	3.4	3.4
ΔAvg.		+0.4	+0.9		+0.2	+0.4		-0.1	+0.1		+0.1	+0.1

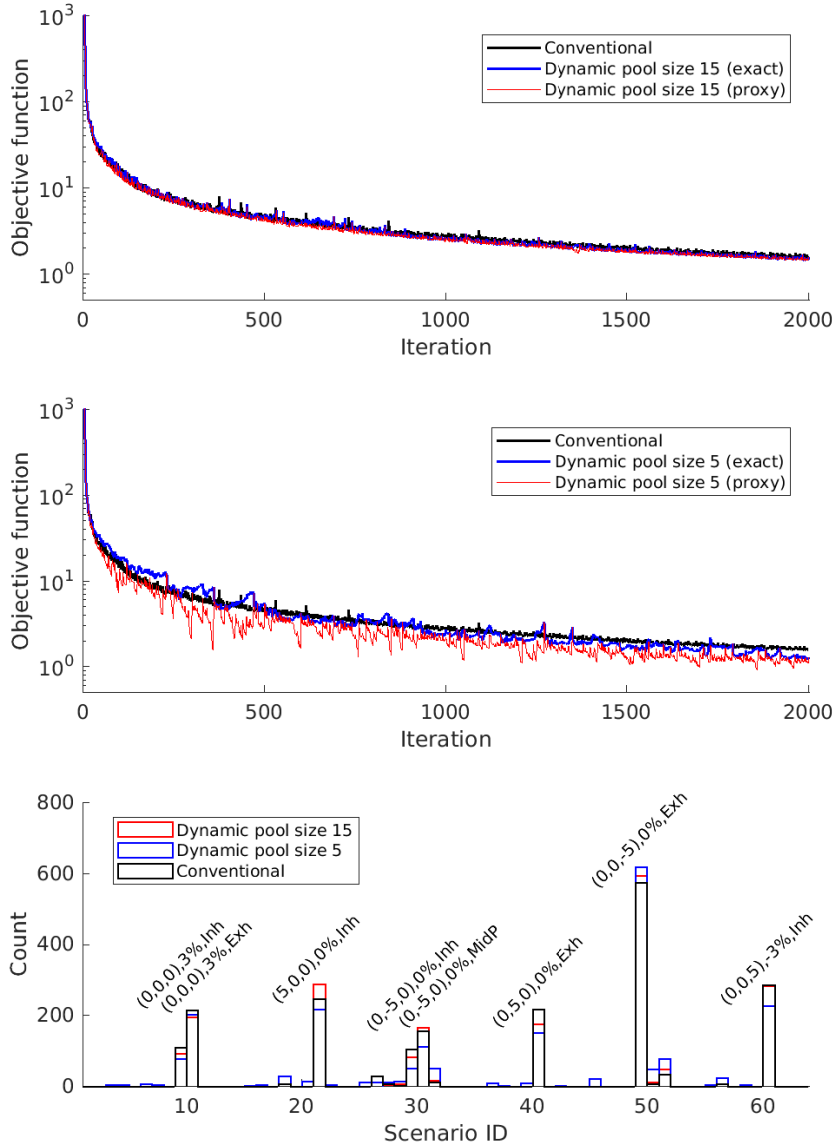


Figure 1: Comparison of *conventional* minimax and *dynamic* minimax optimizations (results of patient P1 are displayed). The top and middle panels show the progression of the (worst-case) objective function value throughout the optimization (top: pool size of $N_A=15$ and middle: pool size of $N_A=5$). For the *dynamic* minimax optimization, the *proxy* worst-case objective function f_{proxy} is displayed in red, whilst the *exact* worst-case objective function f_{exact} is displayed in blue. The bottom panel shows the number of iterations (= counts) that each scenario is evaluated as the worst case. The magnitude of the uncertainties is shown for the most counted scenarios. The uncertainties are displayed as follows: setup error (x,y,z) in mm in the left-right x , anterior-posterior y and superior-inferior z directions, range error and breathing phase (MidP, max inhale or max exhale).

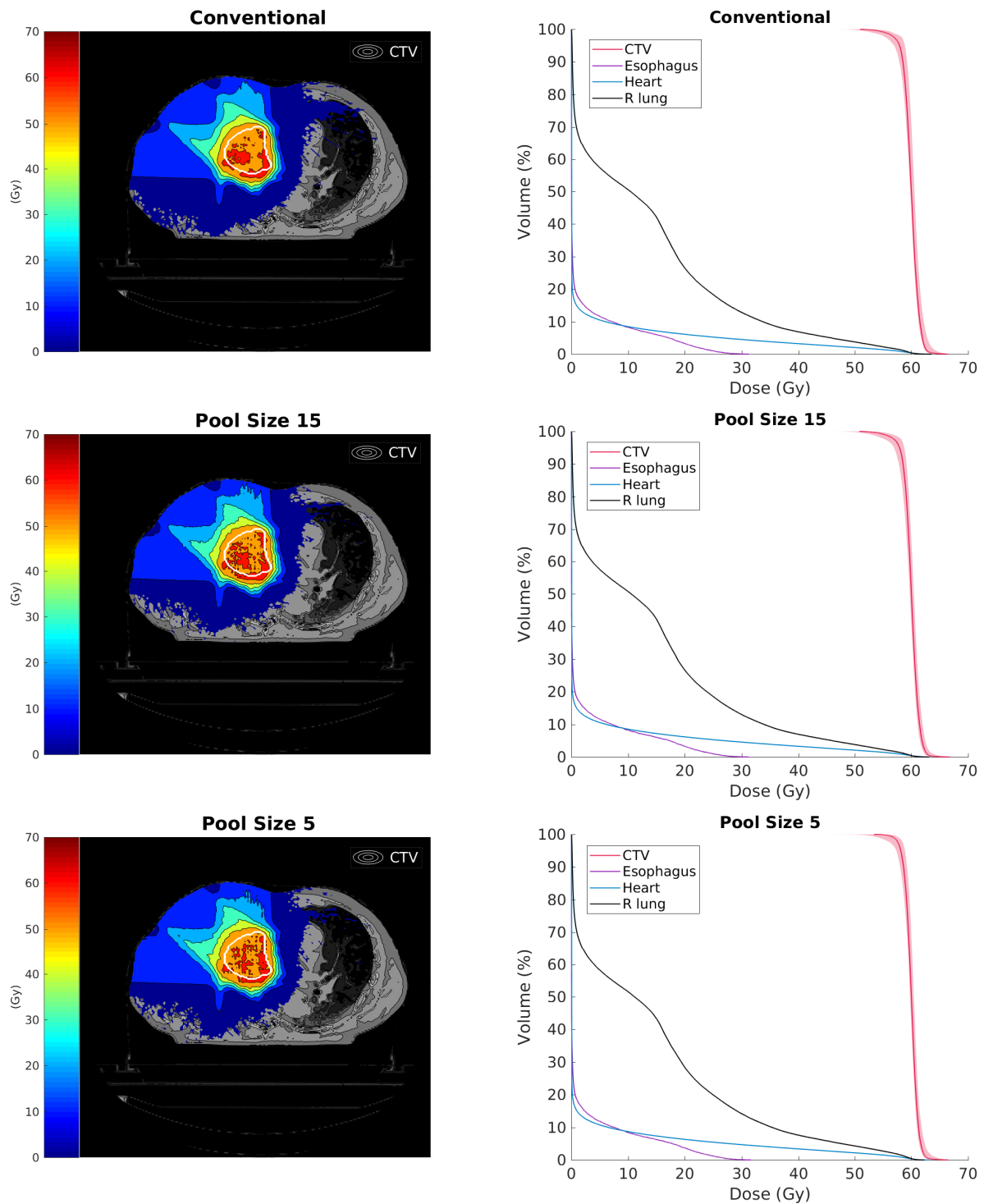


Figure 2: The left column shows the dose distributions for plans obtained using *conventional* minimax optimization and *dynamic* minimax optimization with pool sizes of $N_A=5$ and $N_A=15$ for patient P1. In each figure, the CTV is indicated in white. The right column shows the corresponding DVHs with the CTV-DVH band representing the evaluations in the considered *evaluation* scenarios (see Section II.D.).

289 IV. Discussion

290 In minimax optimization, only the current worst-case scenario is used to guide the optimization
 291 solution. In the meantime, as noted by Fredriksson *et. al.*,¹⁴ minimax algorithms tend to neglect
 292 so-called ‘easy’ scenarios, that is, scenarios where there is little conflict between organ sparing
 293 and target coverage in the objective function. Hence, a substantial amount of computation time
 294 and resources are potentially wasted on scenario evaluations that are rarely the worst case. Fig.
 295 1 (bottom) illustrates this feature of minimax optimization by showing that the optimizer only
 296 accesses a fraction of the full uncertainty set in order to reach its final solution. This suggests that
 297 the majority of scenarios produce either comparable dose distributions or produce dose distributions
 298 where the planning objectives are consistently well respected. Fredriksson argues that disregarding
 299 ‘easy’ scenarios is one of the main disadvantages of the minimax algorithm when comparing it
 300 to other classes of robust optimization algorithms.¹⁴ In fact, it is exactly this drawback that the
 301 *dynamic* minimax algorithm attempts to address. By relying on the sparsity of active scenarios in
 302 the solution space, fewer scenarios are needed whilst still preserving most of the information of the
 303 full problem. In doing so, the computational cost of an iteration is significantly reduced (in other
 304 words, the number of scenario evaluations performed at each iteration is reduced), resulting in an
 305 accelerated optimization process (a time gain of up to 84% is obtained).

306 The optimization curves in Section III.A. show that by reducing the size of the active pool
 307 N_A , the optimization noise level increases. Fundamentally, worst-case robust optimization is in-
 308 herently a noisy optimization process. This is explained by the fact that different optimization
 309 scenarios are used throughout the optimization as a result of the discontinuous *max* operator (see
 310 Eq. 1). Additionally, the projection method (see Section II.C.), to handle constraints on the op-
 311 timization variables (the spot weights), also adds noise to the optimization. In addition to the
 312 above-mentioned noise sources, the *dynamic* minimax algorithm, will add optimization noise by
 313 regularly changing the possible optimization scenarios throughout the optimization process. This
 314 effect will be more pronounced for smaller active pool sizes, which change their composition more
 315 frequently. The additional noise level produced by the *dynamic* minimax algorithm is exemplified in
 316 Fig. 1 (bottom). As shown, optimizations with smaller pool sizes will explore an increased number
 317 of scenarios in the solution space. By increasing the pool size slightly (to $N_A = 15$), the noise is
 318 reduced to a level comparable in magnitude to the *conventional* minimax optimization. However,
 319 as the results of Section III.B. indicate, the increased optimization noise level does not harm the

320 final quality of the treatment plans. In fact, results indicate that a noisy optimization trajectory in
321 the solution space might be advantageous in order to further explore and eventually find a better
322 solution; this is an approach commonly employed in simulated annealing and stochastic gradient
323 descent optimization schedules.

324 The *dynamic* minimax algorithm was tested for 4D-robust optimization of lung tumor cases
325 with motion. Moving lung tumor cases typically present difficulties in terms of generating robust
326 treatment plans with acceptable plan quality, hence these cases were chosen to test the proposed
327 method. The *dynamic* minimax optimization could be applied to 3D-robust optimization, however,
328 the time-gain is expected to be less significant since 3D-robust optimization typically uses less
329 uncertainty scenarios for its optimization.

330 In order to further validate the optimality of the proposed the pool size, the algorithm should
331 be tested for a wider set of patient cases. For instance, in highly complex cases (i.e., large tumor
332 motion with considerable conflicts among the planning objectives), it is recommended to employ
333 a more conservative approach by using a larger the active pool size. This would guarantee that
334 important scenarios are not missed throughout the optimization. Based on the results of the present
335 study, by using a pool size of 15, almost equal results are obtained as for the *conventional* minimax
336 whilst still achieving a significant plan optimization time gain of 67%. As a future perspective,
337 instead of a fixed pool size, an adaptive pool size could be considered which could identify the
338 necessary number of active pool scenarios. By adapting the active pool size over time, such an
339 *adaptive dynamic* minimax algorithm should be able to handle automatically those cases where
340 numerous scenarios contribute equally in the optimization.

341 It must be noted that this study only focuses on reducing the optimization time and does not
342 deal with other computational aspects (such as the memory consumption) of minimax optimization.
343 In particular, the computation of the beamlet dose-influence matrices gives a large contribution
344 to the overall plan computation time (especially for Monte Carlo-based dose computations). The
345 following solutions exist that can reduce the dose computation time and which could potentially be
346 used in conjunction with the *dynamic* minimax optimization: first, the number of beamlet dose-
347 influence matrices can be reduced by performing a pre-selection of relevant uncertainty scenarios,¹⁸
348 and second, a hybrid Monte Carlo-pencil beam dose optimizer can be used to accelerate the plan
349 computation time with Monte-Carlo like accuracy.²¹

V. Conclusions

In minimax optimization, the dose distributions must be evaluated for all uncertainty scenarios in order to evaluate their respective objective functions. As a result, the plan optimization time linearly scales with the number of pre-defined uncertainty scenarios. Especially for lung tumor patients, which need a large number of scenarios to robustly optimize their treatment plans, the associated computational burden may cause excessive plan computation times. This issue limits the use of robust optimization in the clinical environment.

In this study, we propose an approximate worst-case robust optimization algorithm that accelerates minimax optimization. The proposed *dynamic* minimax algorithm relies on the fact that minimax algorithms neglect so-called ‘easy’ scenarios where there is little conflict among the planning objectives. Therefore, instead of evaluating all scenarios in the pre-defined uncertainty set, only a reduced set of active pool scenarios is considered. Following stochastic annealing optimization schedules, these active scenarios are updated according to a variable called the ‘acceptance probability set’. This variable expresses the probability that a scenario might be evaluated as the worst case. By doing so, only the scenarios that are contributing most to the optimization, at that moment, will be retained and accessible in order to guide the optimization solution. [The proposed method was applied to 4D-robust minimax optimization and tested for six moving lung tumor cases. Results show that](#), on average, an optimization time gain of up to 84% is achieved without compromising either target robustness or normal tissue sparing.

Acknowledgements

Gregory Buti is supported by the Télévie Grant from the Belgian ‘Fonds National pour la Recherche Scientifique’ F.R.S-FNRS (Grant No. 7453918F). Computational resources have been provided by the supercomputing facilities of the Université Catholique de Louvain (CISM/UCL) and the Consortium des Équipements de Calcul Intensif en Fédération Wallonie Bruxelles (CÉCI) funded by the F.R.S.-FNRS under convention 2.5020.11. Kevin Souris is funded by the Walloon region (MECATECH/BIOWIN, Grant No. 8090). Ana M. Barragán Montero is funded by the Walloon region (PROTHERWAL/CHARP, Grant No. 7289). Marie Cohilis is supported by the Télévie Grant from the F.R.S-FNRS (Grant No. 7450517F). John A. Lee is a Senior Research Associate with the F.R.S.-FNRS.

380

379 **References**

- 381 ¹ A. Elhammali, P. Blanchard, A. Yoder, Z. Liao, X. Zhang, X. R. Zhu, P. K. Allen, M. Jeter,
382 J. Welsh, and Q.-N. Nguyen, Clinical outcomes after intensity-modulated proton therapy
383 with concurrent chemotherapy for inoperable non-small cell lung cancer, *Radiotherapy and*
384 *Oncology* **136**, 136–142 (2019).
- 385 ² N. Nakamura, K. Hotta, S. Zenda, H. Baba, S. Kito, T. Akita, A. Motegi, H. Hojo, M. Naka-
386 mura, R. V. Parshuram, M. Okumura, and T. Akimoto, Hypofractionated proton beam ther-
387 apy for centrally located lung cancer, *Journal of Medical Imaging and Radiation Oncology* **63**,
388 552–556 (2019).
- 389 ³ R. M. Hoshina, T. Matsuura, K. Umegaki, and S. Shimizu, A Literature Review of Proton
390 Beam Therapy for Prostate Cancer in Japan, *Journal of Clinical Medicine* **8**, 48 (2019).
- 391 ⁴ P. C. Park, J. P. Cheung, X. R. Zhu, A. K. Lee, N. Sahoo, S. L. Tucker, W. Liu, H. Li,
392 R. Mohan, L. E. Court, and L. Dong, Statistical Assessment of Proton Treatment Plans Under
393 Setup and Range Uncertainties, *International Journal of Radiation Oncology*Biophysics*
394 **86**, 1007–1013 (2013).
- 395 ⁵ S. Brousmiche, K. Souris, J. O. de Xivry, J. A. Lee, B. Macq, and J. Seco, Combined influence
396 of CT random noise and HU-RSP calibration curve nonlinearities on proton range systematic
397 errors, *Physics in Medicine & Biology* **62**, 8226–8245 (2017).
- 398 ⁶ A. J. Lomax, Intensity modulated proton therapy and its sensitivity to treatment uncertainties
399 1: the potential effects of calculational uncertainties, *Physics in Medicine and Biology* **53**,
400 1027–1042 (2008).
- 401 ⁷ A. J. Lomax, Intensity modulated proton therapy and its sensitivity to treatment uncertainties
402 2: the potential effects of inter-fraction and inter-field motions, *Physics in Medicine and Biology*
403 **53**, 1043–1056 (2008).
- 404 ⁸ W. Liu, X. Zhang, Y. Li, and R. Mohan, Robust optimization of intensity modulated proton
405 therapy, *Medical Physics* **39**, 1079–1091 (2012).
- 406 ⁹ D. Pflugfelder, J. J. Wilkens, and U. Oelfke, Worst case optimization: a method to account for
407 uncertainties in the optimization of intensity modulated proton therapy, *Physics in Medicine*
408 *and Biology* **53**, 1689–1700 (2008).

- 409 ¹⁰ A. Fredriksson, A. Forsgren, and B. Hårdemark, Minimax optimization for handling range and
410 setup uncertainties in proton therapy, *Medical Physics* **38**, 1672–1684 (2011).
- 411 ¹¹ J. Unkelbach, T. Bortfeld, B. C. Martin, and M. Soukup, Reducing the sensitivity of IMPT
412 treatment plans to setup errors and range uncertainties via probabilistic treatment planning,
413 *Medical Physics* **36**, 149–163 (2008).
- 414 ¹² A. Fredriksson, A characterization of robust radiation therapy treatment planning methods-
415 from expected value to worst case optimization, *Medical Physics* **39**, 5169–5181 (2012).
- 416 ¹³ J. Unkelbach, M. Alber, M. Bangert, R. Bokrantz, T. C. Y. Chan, J. O. Deasy, A. Fredriksson,
417 B. L. Gorissen, M. van Herk, W. Liu, H. Mahmoudzadeh, O. Nohadani, J. V. Siebers, M. Witte,
418 and H. Xu, Robust radiotherapy planning, *Physics in Medicine & Biology* **63**, 22TR02 (2018).
- 419 ¹⁴ A. Fredriksson and R. Bokrantz, A critical evaluation of worst case optimization methods for
420 robust intensity-modulated proton therapy planning, *Medical Physics* **41**, 081701 (2014).
- 421 ¹⁵ L. V. van Dijk, R. J. H. M. Steenbakkers, B. ten Haken, H. P. van der Laan, A. A. van ‘t
422 Veld, J. A. Langendijk, and E. W. Korevaar, Robust Intensity Modulated Proton Therapy
423 (IMPT) Increases Estimated Clinical Benefit in Head and Neck Cancer Patients, *PLOS ONE*
424 **11**, e0152477 (2016).
- 425 ¹⁶ D. Cummings, S. Tang, W. Ichter, P. Wang, J. D. Sturgeon, A. K. Lee, and C. Chang, Four-
426 dimensional Plan Optimization for the Treatment of Lung Tumors Using Pencil-beam Scanning
427 Proton Radiotherapy, *Cureus* (2018).
- 428 ¹⁷ K. Bernatowicz, X. Geets, A. Barragan, G. Janssens, K. Souris, and E. Sterpin, Feasibility of
429 online IMPT adaptation using fast, automatic and robust dose restoration, *Physics in Medicine
430 & Biology* **63**, 085018 (2018).
- 431 ¹⁸ G. Buti, K. Souris, A. M. B. Montero, J. A. Lee, and E. Sterpin, Towards fast and robust 4D
432 optimization for moving tumors with scanned proton therapy, *Medical Physics* (2019).
- 433 ¹⁹ S. Kirkpatrick, C. D. Gelatt, and M. P. Vecchi, Optimization by Simulated Annealing, *Science*
434 **220**, 671–680 (1983).
- 435 ²⁰ A. M. B. Montero, Miropt - <http://www.openmiropt.org/> Accessed November 2019.
-

- 436 ²¹ A. M. B. Montero, K. Souris, D. Sanchez-Parcerisa, E. Sterpin, and J. A. Lee, Performance of a
437 hybrid Monte Carlo-Pencil Beam dose algorithm for proton therapy inverse planning, *Medical*
438 *Physics* **45**, 846–862 (2017).
- 439 ²² K. Souris, MCSquare - <http://www.openmcsquare.org/> Accessed June 2019.
- 440 ²³ S. Huang, M. Kang, K. Souris, C. Ainsley, T. D. Solberg, J. E. McDonough, C. B. Simone, and
441 L. Lin, Validation and clinical implementation of an accurate Monte Carlo code for pencil beam
442 scanning proton therapy, *Journal of Applied Clinical Medical Physics* **19**, 558–572 (2018).
- 443 ²⁴ K. Souris, A. B. Montero, G. Janssens, D. D. Perri, E. Sterpin, and J. A. Lee, Technical Note:
444 Monte Carlo methods to comprehensively evaluate the robustness of 4D treatments in proton
445 therapy, *Medical Physics* (2019).
- 446 ²⁵ H. Paganetti, Range uncertainties in proton therapy and the role of Monte Carlo simulations,
447 *Physics in Medicine and Biology* **57**, R99–R117 (2012).
- 448 ²⁶ M. Wanet, E. Sterpin, G. Janssens, A. Delor, J. A. Lee, and X. Geets, Validation of the
449 mid-position strategy for lung tumors in helical TomoTherapy, *Radiotherapy and Oncology*
450 **110**, 529–537 (2014).
- 451 ²⁷ G. Janssens, OpenReggui - <https://www.openreggui.org/> Accessed June 2019.
- 452 ²⁸ T. Inoue, J. Widder, L. V. van Dijk, H. Takegawa, M. Koizumi, M. Takashina, K. Usui,
453 C. Kurokawa, S. Sugimoto, A. I. Saito, K. Sasai, A. A. van't Veld, J. A. Langendijk, and E. W.
454 Korevaar, Limited Impact of Setup and Range Uncertainties, Breathing Motion, and Interplay
455 Effects in Robustly Optimized Intensity Modulated Proton Therapy for Stage III Non-small
456 Cell Lung Cancer, *International Journal of Radiation Oncology*Biophysics* **96**, 661–669
457 (2016).